Ionic Liquid Induced All-α to α+β Conformational Transition in Cytochrome c with Improved Peroxidase Activity in Aqueous Medium

Pankaj Bharmoria,[a] Tushar J Trivedi[b], Ashok Pabbathi[c], Anunya Samanta,[c] and Arvind Kumar,[*,a,d]

[a]*Academy of Scientific and Innovative research (AcSIR), Central Salt and Marine Chemicals Research Institute, Council of Scientific and Industrial Research (CSIR), G. B. Marg, Bhavnagar-364002, Gujarat, India.*

[b]*Graduate School of EEWS (Energy Environment Water Sustainability), KAIST, 291 Daehak-ro, Yuseong Gu, Daejeon 305-701, Republic of Korea.*

[c]*School of Chemistry, University of Hyderabad, Hyderabad 500 046, India*

[d]*Salt and Marine Chemical Discipline, Central Salt and Marine Chemicals Research Institute, Council of Scientific & Industrial Research (CSIR), G. B. Marg, Bhavnagar-364002, Gujarat, India.*

Corresponding Authors

arvind@csmcri.org (A. Kumar); Tel +91-278-2567039; Fax: +91-278-2567562

Abstract

Choline dicotylsulfosuccinate [Cho][AOT] (a surface active ionic liquid) has been found to induce all-α to α+β conformational transition in the secondary structure of enzyme cytochrome c (Cyt c) with an enhanced peroxidase activity in aqueous vesicular phase at pH 7.0. [Cho][AOT] interacted with Cyt c distinctly at three critical concentrations (aggregation C_1, saturation C_2 and vesicular C_3) as detected from isothermal titration calorimetric analysis. Oxidation of heme iron was observed from the disappearance of Q band in UV-Vis spectra of Cyt c upon [Cho][AOT] binding post C_3. Circular dichroism analysis (CD) has shown the loss in both secondary (190-240 nm) and tertiary (250-300 nm) structure of Cyt c in the monomeric regime till C_1, followed by their stabilization till the pre-vesicular regime ($C_1 \rightarrow C_3$). Loss in both secondary and tertiary structure has been observed in the post vesicular regime with the change in Cyt c conformation from all-α to α+β which is similar to the conformational changes of Cyt c upon binding with mitochondrial membrane (*Biochemistry* **1998**, *37*, 6402-6409) thus citing the potential utility of [Cho][AOT] membranes as an artificial analog for in vitro bio-mimicking. Fluorescence correlation spectroscopy (FCS) measurements confirm unfolding of Cyt c in the vesicular phase. Dynamic light scattering experiments have shown the contraction of [Cho][AOT] vesicles upon Cyt c binding driven by electrostatic interactions observed by charge neutralization from zeta potential measurements. [Cho][AOT] has been found to enhance the peroxidase activity of Cyt c with maximum activity at C_3, observed by using 2,2'-Azino-bis(3-ethylbenzothiazoline-6-sulfonic acid) diammonium salt as substrate in the presence of hydrogen peroxide. The result shows relevance of ionic liquids tuning to surfactants for bio-mimicking of specific membrane protein-lipid interactions.

1. Introduction

The eternal synergism of lipid-proteins interactions in nature has attracted researchers to mimic them in vitro in sight of possible applications as biological membrane-protein analog.[1-5] The synergic interaction of cytochrome c (Cyt c) with inner membrane of mitochondria during electron transport chain is one such example where it carries one electron between complex III (Coenzyme Q - Cyt c reductase) and complex IV (Cyt c oxidase) which drives the formation of adenosine triphosphate (ATP). Cyt c is a 104 amino acids long globular heme protein with all-α secondary structural conformation wherein the strong field histidine His (18) and methionine Met (80) coordination at axial positions stabilizes its low spin state.[6-8] In eukaryotes Cyt c is found attached to the inner membrane of mitochondrion which is composed of a phosphatidyl choline bilayer and undergoes conformational transition during apoptosis. In the present manuscript we have attempted to mimic these interactions in vitro with a horse heart Cyt c and an ionic liquid surfactant, choline dioctylsulfosuccinate ([Cho][AOT]) in aqueous media at the physiological pH. Inspiration of the present work has been kicked by the growing interest of scientific community in surface active ionic liquids (SAILs) for various surfactant based application, specifically SAILs-proteins colloidal formulations. Surfactant-proteins formulations have immense commercial applications in pharmaceuticals, cosmetics, paints, coatings, detergents, bioelectronics and biochemical reactions.[9-11] Although there is no hardliner difference in literature but SAILs are differentiated from conventional ionic surfactants in terms of their low melting point (<100^{o}C), usually superior surface activity, green nature (depending upon choice of cations/anions), and structural tunability.[12-23] [Cho][AOT] (melting point = -47.4^{o}C) is a room temperature surface active ionic liquid and has been reported in detail for its aggregation behavior in aqueous media in our earlier article.[19]

In lieu of SAILs exploration as potential alternative of conventional surfactants for surfactant-protein formulation they have been investigated with protein like BSA, HSA and cellulase in aqueous media.[24-32] Among these reports the 1-tetradecyl-3-methylimidazolium bromide,[24-25] 3-methy-1-octylimidazolium dodecylsulfate, 3-methyl-1-octylimidazolium chloride,[26] 3-methyl-1-(ethoxycarbonylmethyl)imidazolium dodecylsulfate, and 3-methyl-1-(ethoxycarbonylmethyl)pyrrolidinium dodecylsulfate[28] and 3-decyl-1-methylimidazolium bromide[29] have been reported to induce significant alteration in the tertiary structure of BSA at low concentration below *cmc* and imidazolium head group was found to be more denaturing as compared to pyrrolidinium head group.[28] Whereas the biamphiphillic ionic liquid (BAIL), 1-3-methy-1-octylimidazolium dodecylsulfate has been reported to induce refolding of BSA after initial unfolding at very low concentration and stabilized it against aggregation in the post vesicular regime.[30] As far as other proteins are concerned, 3-methy-1-octylimidazolium dodecylsulfate has been reported to stabilize structure and functional activity of enzyme cellulase.[31] Pharmaceutical SAILs, cetylpyridinium salicylate and benzethonium salicylate have been reported to quench the fluorescence of human serum albumin and bind strongly to its hydrophobic sites.[32] In a recent report Cao et al. have investigated interfacial behavior of protein β-casein and lysozyme in the presence of SAIL, cetylimidazolium bromide and found that at high concentration of surfactant the surfactant and β-casein coadsorb at the interface whereas lysosome molecule gets desorb from the interface due to competitive adsorption.[33] Huang et al. have reported the destruction of the pepsin compact structure at high concentration of cetylimidazolium bromide at decane–water interface.[34] Exploration of SAIL-protein colloidal formulations from commercial point of view requires investigations between more proteins and new SAILs.

Herein, we have investigated the conformational alterations in enzyme Cyt c (a membrane protein) upon binding with a surface active ionic liquid [Cho][AOT] at 298.15 K and pH 7.0 using various physicochemical and spectroscopic techniques. Although there are no reports of Cyt c interaction with SAILs but reports on Cyt c interactions with conventional surfactant exists.[35-40] Anionic surfactants sodium dodecylsulfate (SDS) and sodium bis(2-ethylhexyl)sulfosuccinate (NaAOT) have been reported to induce similar alterations in the secondary structure of Cyt c while altering the heme environment differently. [NaAOT] changed the native low spin Cyt c to denatured low spin Cyt c upon shifting to micellar phase whereas SDS changed the native low spin Cyt c to mixed-spin Cyt c in micellar phase.[35] Chattopadhyay et al. have reported the stabilization of partially folded Cyt c at the sub-micellar concentration of SDS.[36] In fact the interactions of Cyt c with phosphatidylcholine are also reported from fluorescence resonance energy transfer technique and ITC.[37-38]Authors have reported that Cyt c interacts electrostatically with phosphatidylcholine at neutral pH and via hydrogen bonding at the acidic pH.[37] The location of Cyt c was found to be at the lipid-water interface both in complexes at neutral pH and below 6.0.[38] From the ITC studies Dimitrova et al. have reported that the side chain of Cyt c penetrates into the interface region of the bilayer of phosphatidyl choline liposome along with the surface electrostatic interactions with the liposomes negative head group and lysine residues of Cyt c around heme cleft.[39] In an another experiment Zhang et al. have reported that the liposome of a negatively charged dioleoylphosphatidylglycerol interacts endothermically with Cyt c at pH 7.8.[40]

In the present paper [Cho][AOT]-Cyt c binding isotherm from monomeric to post-aggregation regime has been defined from isothermal titration calorimetry (ITC) technique. Alterations in the secondary and tertiary structure of the Cyt c upon [Cho][AOT] binding have been investigated from circular dichroism (CD) spectroscopy. [Cho][AOT] induced changes in the vicinity of heme cleft and oxidation state of the iron center have been detected from UV-Vis spectroscopy. Variations in the hydrodynamic radii of Cyt c upon interaction with [Cho][AOT] have been investigated by performing fluorescence correlation spectroscopy (FCS) measurements on Alexa Fluor488 carboxylic acid dye-labeled Cyt c. The stability and neutralization of vesicle charge upon Cyt c binding were investigated by zeta potential measurements. Size of the vesicle-Cyt c lipoplex has been measured from dynamic light scattering (DLS). Peroxidase activity of Cyt c in the absence and presence of [Cho][AOT] was analyzed from UV-Vis spectra of 2,2'-Azino-bis(3-ethylbenzothiazoline-6-sulfonic acid) diammonium salt as substrate and hydrogen peroxide as oxygen donor.

2. Experimental

2.1 Materials.

Enzyme Cytochrome c (horse heart) was purchased from SRL Pvt. Ltd. and was characterized for purity using spectroscopic techniques. The prominent bands at 409, 528 and 549 nm in the UV-Vis spectra and 40.1% α-helical content in far-UV CD spectra in Millipore water and phosphate buffer pH 7.0 validated the purity of enzyme (Fig. S1, ESI†). Dioctyl sodium sulfosuccinate (AOT) (>99%) was purchased from sd fine-chem Ltd. Choline chloride (≥98%) was purchased from Sigma-Aldrich. Both the chemicals were AR grade and used as received. Ionic liquid choline dioctylsulfosuccinate, was synthesized as per the procedure published in our earlier article.[19] The synthesized [Cho][AOT] was characterized using ^{1}H-NMR (Fig. S2 ESI†) and LCMS (ESI†). The melting point (-47.4^{o}C) of [Cho][AOT] was measured from differential scanning calorimetry (Fig. S3 ESI†). 2,2'-Azino-bis(3-ethylbenzothiazoline-6-sulfonic acid) diammonium salt (ABTS) (>99%) was purchased from Sigma-Aldrich. Hydrogen peroxide (H_2O_2) 30% (w/v) was purchased from Fischer Scientific. The dye Alexa Fluor488 carboxylic acid TFP ester was purchased from Invitrogen. The solutions (w/v) of [Cho][AOT] with or without Cyt c were prepared using an analytical balance with a precision of ±0.0001 g (Denver Instrument APX-200) in phosphate buffer (50 mM, pH 7.0). Buffer solution was prepared in degassed Millipore grade water using AR-grade potassium di-hydrogen phosphate (99%) and di-potassium hydrogen phosphate (99%) purchased from sd fine-chem Ltd. The concentration of Cyt c used for this study is 18 μM which is maintained from UV measurements of 409 nm peak with a molar extinction coefficient of 1.06×10^{5} M^{-1}.[31] Stock solution of Cyt c was stored at 4°C. Molecular structure of [Cho][AOT] and model structure of the amino acid sequences of the Cyt c are depicted in Scheme 1.[7]

2.2 Methods.

2.2.1. Isothermal titration calorimetry. Enthalpy changes (dH) due to interaction of [Cho][AOT], with Cyt c in buffer solution were measured at 298.15 K using MicroCal ITC200 microcalorimeter, with an instrument controlled Hamiltonian syringe having volume capacity of 40 μL. The titration was done by adding 1.3 μL aliquots of [Cho][AOT] stock solution into the sample cell containing 200 μL of phosphate buffer or 18 μM Cyt c solution with continuous stirring at 500 rpm. The parameters like time of addition and duration between each addition were controlled by the software provided with the instrument. Enthalpy changes at each injection were measured and plotted against the concentration by using origin software provided with the instrument. [Cho][AOT]-Cyt c binding isotherm was used to define various concentration regimes.

2.2.2 UV-Vis spectroscopy. The changes around the heme cleft of Cyt c upon [Cho][AOT] binding in different concentration regimes were measured using UV 3600 Shimadzu UV-Vis-NIR spectrophotometer at 298.15 K. The concentrated solution of [Cho][AOT] was titrated against 18 μM Cyt c aqueous buffer solution in a quartz cuvette of 1 cm path length. The measurements were done after 3 minutes of [Cho][AOT] addition at each concentration in order to match the time gap of energy changes after each addition in ITC analysis. Prior to the measurements the baseline was corrected using phosphate buffer solution as blank.

2.2.3 Circular dichroism spectroscopy. Alterations in the secondary (α-helical and β-sheet) and tertiary structure of Cyt c upon interaction with [Cho][AOT] at different concentrations were monitored through, a Jasco J-815 CD spectrometer at 298.15 K. Spectra were collected in a 1mm path length quartz cuvette at a scan rate of 100 nm per minute and sensitivity of 100 mdeg. The response time and the bandwidth were 2 s and 0.2 nm, respectively. Fresh samples of different concentrations were prepared at the time of measurement in order to avoid the time gap as per VU and ITC measurements.

2.2.4. Fluorescence correlation spectroscopy. FCS was used to analyze the variation of the hydrodynamic radii of Cyt c upon interaction with [Cho][AOT]. For this purpose the protein was first labeled with Alexa Fluor488 carboxylic acid dye and the measurements were carried out on the dye-labeled protein.

2.2.4.1 Protein Labeling. The dye, Alexa 488 TFP ester is conjugated to cytochrome c by following a standard procedure. Briefly, 2:1 molar mixture of the dye and protein was taken in a carbonate buffer (pH 9.2, 0.1 M) and incubated for 2 hrs. Subsequently, the free dye was separated using a sephadex G-25 column equilibrated in phosphate buffer (pH 7.0, 50 mM).

2.2.4.2 Instrumentation. FCS experiments were performed on a time-resolved confocal fluorescence microscope, MicroTime 200 (PicoQuant). An excitation light of 485 nm was reflected by a dichroic mirror and focused onto the sample using water immersion objective (60 X/1.2 NA). The fluorescence from the sample was collected by the same objective and passed through a filter and pinhole before entering the two detectors (single photon avalanche diodes). The correlation curves were generated by cross-correlating the signals from two detectors. For FCS experiments, 100 nM solution of the labeled protein was used. The excitation laser power was ~5 μW and total concentration of protein in the solution was maintained at 18 μM by adding unlabeled protein.

2.2.5. Dynamic light scattering. The size of [Cho][AOT] vesicles and vesicle-Cyt c lipoplex were analyzed at 298.15 K, using a NaBiTec Spectro Size^{TM} 300 light scattering apparatus, Germany) with a He−Ne laser (660 nm, 4 Mw). The hydrodynamic measurements were carried out in a quartz cuvette of 1 cm path length by considering the viscosity and refractive indices of the solutions prepared. The data evaluation of the DLS measurements was performed with the inbuilt CONTIN algorithm. The error observed in the size of native vesicles and lipoplexes was ±8 nm.

2.2.6. Zeta potential measurements. Zeta potential of the native [Cho][AOT] vesicles at different concentrations and Cyt c-[Cho][AOT] lipolexes was measured using Zetasizer Nano ZS light scattering apparatus (Malvern Instruments, UK) with a He-Ne laser (633 nm, 4 Mw). Measurements were done in a DTS1O60 cell having gold coated electrodes at 298.15 K. Prior to the measurements the cell was calibrated with a freshly prepared negatively charged AgI sol whose zeta potential was found to be -38±2 mV. Zeta potential (ζ) of colloidal particles is a measure of their stability and surface charge. It is a potential difference between the plane of shear and Guoy Chapman layer. The instrument measures the electrophoretic mobility of the particles under the applied electric field and finally gives ζ using Smoluchowski equation, ($\zeta = 4\pi\eta\mu / \varepsilon$).

2.2.7. Atomic force microscopy. Atomic force microscopy (AFM) imaging was performed using Ntegra Aura atomic force microscope (NT-MDT, Russia) in a semi-contact mode using an NSG-01 silicon probe. Samples were prepared by putting a drop of the sample solution on thin mica sheet and dried in air.

2.2.8. Peroxidase activity of Cyt c. Peroxidase activity of the cytochrome c was analyzed using ABTS/H_2O_2 system wherein Cyt c catalysed the oxidation of ABTS in the presence of H_2O_2 and produces green color $ABTS^{\bullet+}$ radical. The formation of $ABTS^{\bullet+}$ was monitored by changes in absorption spectra at 417 nm and intensity of the green color. The absorption spectra of mixtures composed of 2 μM Cyt c + 1 mM H_2O_2 + 3mM ABTS at 0, 0.13, 0.4 and 2 $mmol.L^{-1}$ concentrations of [Cho][AOT] were taken at an interval of 20 seconds for 330 seconds. Before UV analysis the 2 μM Cyt c + 1 mM H_2O_2 mixture was incubated for 1 minute with consequent addition of ABTS and further incubation of the reaction mixture for 30 seconds.

3. Results and Discussion

3.1. Binding isotherm of [Cho][AOT] to cytochrome c. The stepwise binding of [Cho][AOT] to Cyt c at 298.15 K was monitored from ITC experiments.[41] Fig. 1 shows the thermograms of [Cho][AOT] aggregation in buffer, Cyt c solution and binding to Cyt c. The corresponding differential power (dP) plots are shown in Fig. S4 (ESI†). The aggregation of [Cho][AOT] in buffer solution is mostly endothermic and switched to exothermic at 0.6 $mmol.L^{-1}$ in the vesicle rich region. The critical vesicular concentration (CVC) in the buffer and Cyt c solution was found to be 0.34 $mmol.L^{-1}$ and 0.40 $mmol.L^{-1}$ respectively. The formation of vesicles has also been observed by atomic force microscopy (Fig. S5 ESI†) and DLS analysis (discussed later). Aggregation in the Cyt c solution at a slight higher concentration indicates [Cho][AOT] binding to Cyt c. The thermodynamic parameters such as standard enthalpy of aggregation (ΔH^{o}_{agg}) and standard entropy of aggregation (ΔS^{o}_{agg}) obtained by fitting the thermograms using instrument inbuilt fitting software and the Gibbs free energy of aggregation (ΔG^{o}_{agg}) obtained from ΔH^{o}_{agg} and ΔS^{o}_{agg} values using Gibbs Helmholtz equation ($\Delta G^{o}_{agg} = \Delta H^{o}_{agg} - T\Delta S^{o}_{agg}$) are tabulated in Table 1. The high negative value of ΔG^{o}_{agg} has demonstrated the feasibility of aggregation. The ΔH^{o}_{agg} in buffer and Cyt c solution were found to be -4.79 and -6.05 $kJ.mol^{-1}$. Comparing the enthalpy and entropy contribution to free energy from Table 1 it has been found that aggregation process is entropy driven.

The [Cho][AOT]→Cyt c binding isotherm (Fig. 1, Subtracted) is composed of four interaction regimes (1) monomeric (0-0.13 mmol.L^{-1}), (2) aggregation (0.13-0.28 mmol.L^{-1}), (3) pre-vesicular (0.28-0.4 mmol.L^{-1}) and (4) post vesicular (≥ 0.4 mmol.L^{-1}). Unlike other charged surfactant-protein systems[30-31] the binding of [Cho][AOT] to Cyt c is mostly endothermic except in the vesicle rich region. In the monomeric regime, $[Cho]^+$ and $[AOT]^-$ ions binds to the various charged sites on Cyt c till 0.13 mmol.L^{-1} defined as critical aggregation concentration C_1. The hydrophobic interactions among the ions adsorbed at various sites on the Cyt c drives the formation of Cyt c-[Cho][AOT] aggregate complexes upon increasing the concentration beyond C_1. The Cyt c induced aggregation of [Cho][AOT] is accompanied by the decrease in enthalpy and continues till the Cyt c gets saturated at 0.28 mmol.L^{-1} (critical saturation concentration, C_2). The enthalpy changes due to the binding of [Cho][AOT] to Cyt c at C_1 and C_2 were found to be 1.46 kJ.mol^{-1} and 0.78 kJ.mol^{-1}. In the pre-vesicular regime various Cyt c molecules interacts with each other due to sharing of [Cho][AOT] aggregates till C_3. Enthalpy change at C_3 was found to be 1.95 kJ.mol^{-1}. In the post vesicular regime the [Cho][AOT] vesicles interacts with Cyt c with the decrease in enthalpy till 0.65 mmol.L^{-1}, beyond which the enthalpy changes became almost constant. To further investigate the individual contribution of the ionic liquid moieties towards Cyt c binding we investigated binding of [Cho][Cl] and [NaAOT] to Cyt c till 0.13 mmol.L^{-1}. (Fig. S6 (A) and (B), ESI†). The combined binding enthalpy (1.256 kJ.mol^{-1}) of [Cho][Cl] and [NaAOT] to Cyt c till C_1 (0.13 mmol.L^{-1}) is comparable to that of [Cho][AOT]-Cyt c binding (dH = 1.46 kJ.mol^{-1}) and .[NaAOT] has major contribution (1.226 kJ.mol^{-1}) compared to [Cho][Cl] (0.030 kJ.mol^{-1}) to the total enthalpy change. These observations shows that AOT anion has a more binding affinity for Cyt c compared to cholinium cation until C_1 of [Cho][AOT]-Cyt c binding isotherm is arrived at.

3.2. Alterations of cytochrome c conformation around the heme cleft

The UV-Vis spectra of Cyt c at different concentrations of [Cho][AOT] are shown in Fig. 2 (A) and (B). For better clarity the spectra have been divided into two regions, 380 to 440 nm and 450-650 nm. The combined spectra are provided in Fig. S7 (ESI†). Plots of variation in the intensities of different absorption bands as a function of [Cho][AOT] are shown in Fig. 2C-E. In its native conformation Cyt c shows a number of absorption bands like, 280 nm due to n-π^* transition of aromatic amino acids (Tryptophan, tyrosine, phenylalanine), an intense S_0→S_2, soret band at 409 nm due to π-π^* transition of heme group wherein the iron atom is imposed by axial histidine (His) and methionine (Met) amino acid ligands.[42] A weak $S_0 \rightarrow S_1$ Q band at 528 and 550 nm due to π-π^* transition of heme indicating its reduced form.[42]

The absorbance of peak at 409 nm decreased with the addition of [Cho][AOT] till 0.31 mmol.L^{-1} (around C_2), increased thereafter all through the pre and post vesicular regimes and became almost constant in the vesicle rich region (beyond 0.65 mmol.L^{-1}). The variation in absorbance at 409 nm is accompanied by an increase in absorbance of 528 and 549 nm peaks with the origin of isobestic point at 420 nm and 0.17 mmol.L^{-1} of [Cho][AOT]. The heme cleft of Cyt c is buried inside the packed hydrophobic core of hydrophobic amino acids, having some lysine resides at the adjacent position (Scheme 1B).[7] The decrease in absorbance of 409 nm peak indicates the transition from nonpolar to polar environment around the heme cleft as the hypochromic shifts in UV spectra are observed due to the lowering in energy of π^* orbital driven by stabilization in surrounding polar environment. Since, Cyt c is positively charged at pH 7.0,[36] the AOT anion binds to the lysine residues around the heme cleft and causes perturbation in the existing salt-brigde interactions leading to unfolding around the heme cleft. It has also been demonstrated from the ITC experiments that AOT has major contribution to the binding energy till C_1. Beyond C_1, the [Cho][AOT] molecules begins to aggregate on the Cyt c surface to form Cyt c-[Cho][AOT], aggregate complexes driven by protein-IL and IL-IL cooperative interactions. The decrease in absorbance of 409 nm peak in this regime indicates further exposure of π^* orbital to the polar environment due to unfolding of the protein around the heme cleft which is also supported by a 2 nm bathochromic shift from 409 nm to 411 nm. Das et al. have reported that both polar and non-polar interactions drives the SDS induced unfolding of Cyt c around the heme cleft.[43] Above C_2 in the pre and post vesicular regime an increase in absorbance of 409 nm peak occurs which attained constancy to further change at 0.65 mmol.L^{-1} in the vesicle rich region. The increase in absorbance is possible because of the exposure of π^* orbital of the heme to the non-polar environment due to the interaction with the hydrophobic bilayer structure of [Cho][AOT] under formation in the pre and post vesicular region. A 2 nm hypsochromic shift above C_2 also indicates the exposure of heme π^*orbitals to the nonpolar environment. An increase in absorbance of 528 nm peak also indicates significant conformational alterations around heme group which became stable in the post vesicular region above 0.50 mmol.L^{-1} (Fig. 2B and D). Oxidation of the iron from Fe (II) to Fe (III) in the heme cleft occurred with the beginning of vesicular regime which has been indicated by the disappearance of Q band at 549 nm[44] beyond 0.37 mmol.L^{-1} of [Cho][AOT] (Fig. 2B and E). The disappearance of Q band has been reported either due to the displacement or breaking of strong field methionine residue[44] which maintains d^2sp^3 hybridization of iron in heme complex. In high spin state the iron atom attains closed shell configuration with sp^3d^2 hybridization thus preventing the $d\pi$-π^* back bonding leading to disappearance of Q band. The enthalpy change during Fe (II) to Fe (III) oxidation calculated from ITC was found to be 1.17 $kJ.mol^{-1}$. So in the vesicle rich region Cyt c exists in high spin oxidised form. To clarify the role of individual IL ions towards Cyt c conformational alterations we recorded the UV-Vis spectra of Cyt c in the presence of [ChoCl] and [NaAOT] (Fig. S8, ESI†). After analysing Fig. S8 (ESI†) we have found that the interactions of [ChoCl] with Cyt c are very weak and [NaAOT] plays a major role in the conformational alterations of Cyt c around the heme cleft. This observation is also supported by a low dH contribution of [ChoCl]-Cyt c (0.030 $kJ.mol^{-1}$) system to the overall enthalpy change at C_1 of [Cho][AOT]-Cyt c system (1.46 $kJ.mol^{-1}$). Also the oxidation of Fe (II) to Fe (III) occurs upon binding of Cyt c to the bilayers of AOT as evident from the disappearance of Q band only after C_3.

3.3. Alterations in the secondary and tertiary structural conformation

Circular dichroism (CD) has been used as a tool to investigate the alterations in the secondary (far-UV) and tertiary structure (mid-UV) region of Cyt c. Being major chromophores in proteins, the peptide bonds absorbs the far-UV light to induce various π-π^* and n-π^* transitions and gives characteristic CD band to various secondary structural conformations (α-helical, β-sheet, turn and random coil). Any change in the backbone orientation will affect the optical transition and hence indicate about the changes in the secondary structure of the protein.[45-46] The far-UV CD spectra (190-250 nm) of Cyt c at different transition concentrations of [Cho][AOT]-Cyt c interaction is shown in Fig. 3, and the spectra at the entire concentration range is provided as Fig. S6A (ESI†). The % secondary structural content of Cyt c at various concentrations of [Cho][AOT] was calculated using instrument inbuilt secondary structure analysis software and is tabulated in Table 2. The plots showing variation in α-helical and β-sheet content is shown as inset in Fig. 3 whereas the variation in turn and random coil conformations are plotted in Fig. S6 B (ESI†). The native conformation of Cyt c has a characteristic all-α protein CD spectrum, showing prominent negative bands at 208 nm (π-π^* transition) and 222 nm (n-π^* transition) and contains around 40% helical content.[8,47] The calculated α-helical content (40.2%) is agreeing well with the literature value.[8,47] Qualitatively the $-\theta_{222nm}$ band was monitored to check the variation in α-helical structure (Fig. S10, ESI†).[26,28] The $-\theta_{222nm}$ band decreased in a short mean residual ellipsity ($deg.cm^2.dmol^{-1}$) frame from -10.28 to -7.8 till C_3 and increased thereafter to -9.16 till 0.65

mmol.L^{-1} in the post-vesicular regime while maintaining the all-α CD spectra. These results are complying with the UV results at 409 nm peak. A 2 nm blue shift in the $-\theta_{222nm}$ band beyond 0.55 mmol.L^{-1} indicates the origin of β-sheet structure. In the vesicle rich region $-\theta_{222nm}$ band almost disappeared with the transition of CD spectrum from a characteristic all-α to α+β type protein conformation.[47] For better clarity we analyzed the quantitative variations in the different secondary structural compositions (α-helical, β-sheet, turn and random coil). The % α-helical content decreased slightly to 37.5% in the monomeric regime (Inset Fig. 3) accompanied by a slight increase in both turn and random coil structure (Fig. S9B, ESI†). Majority of the α-helices in Cyt c are located at the C and R termini along with fewer helices in the mid part of the protein around the heme cleft.[7] Initial decrease in % α-helical content possibly occurs around the heme cleft having positively charged lysine residues as major electrostatic binding sites for AOT anion as also observed in UV spectra. The % α-helical content increased extensively in the aggregation regime with a consequent decrease in random coil structure till 0.31 mmol.L^{-1} (around C_2) whereas the turn structure remained almost constant till C_2. An increase in the % α-helical and decrease in the % random coil content indicates the refolding of protein backbone in this regime. This is an interesting observation which counters the generalized view of protein-surfactant chemistry that the protein induced aggregates causes significant unfolding of protein in this regime but also demonstrates the specific nature of proteins toward different ligands.[2] Stabilization of partially folded intermediate state of Cyt c in sub-micellar region of SDS support these results wherein the majority of the secondary structure of Cyt c was reported to be retained.[36] The synergic hydrophobic interactions of AOT alkyl chain with the side chains of hydrophobic amino acid also play a role in the protein stabilization. Beyond C_2 a decrease in turn and increase in random coil structure was observed whereas the % α-helical content increased to 50 % till 0.45 mmol.L^{-1} and decreased steeply thereafter in the vesicle rich region to around 13% constant value. An increase in random coil and decrease in α-helical content of protein signifies the unfolding of protein backbone. The decrease in α-helical content in the post vesicular region is also followed by a rise of β-sheet conformation which increased steeply from 15% at 0.65 mmol.L^{-1} to around 39% in the high vesicle rich region. So in the vesicular rich region the Cyt c exist in α+β type protein conformation[47] wherein the signatory α-helical band at $-\theta_{222nm}$ almost diminishes. These results strongly find support from the report that Cyt c binding to mitochondrial membrane decreases its α-helical content by 70-79% and increases its β-sheet up to 135%.[48] Authors have also reported the α+β type CD spectra of

Cyt c upon binding to mitochondrial membrane.[48] The present results shows the potential of [Cho][AOT] bilayers for in vitro bio-mimicking of membrane-protein interactions. We further checked the effect of [ChoCl] and [NaAOT] on the secondary structure of Cyt c (Fig. S11A and B, ESI†) and found that the major secondary structural alterations in Cyt c-[Cho][AOT] system are induced by [AOT] anion and choline acts only as a membrane stabilizer.

Since the fluorescence of Trp residue is quenched by the iron atom of heme cleft,[44] we avoided the fluorescence spectra and monitored the tertiary structural alteration in Cyt c from the near-UV CD spectra (250-300 nm). The tertiary structure of proteins is mainly maintained by non-specific interactions of the side chains of amino acids in the peptide backbone via hydrophobic forces. Cyt c has five tyrosine (Tyr), four phenylalanine (Phe), one tryptophan (Trp), and one thioether linkage, which contribute to the mid-UV CD spectra.[7] The mid-UV CD spectra of Cyt c shows band at 265 nm due to Tyr, at 276 nm due to Phe and at 291 nm due to Trp residue.[36,46] We have analyzed the variation in mean residue ellipsity ($-\theta$) of these bands (Fig. 4) to assess the tertiary structural alterations in Cyt c. The original mid-UV CD spectra are shown in Fig. S12 (ESI†). The $-\theta$ of Trp and Tyr residues decreased initially in the monomeric regime indicating the loss of tertiary structure due to protein unfolding driven by site specific binding of [Cho][AOT] monomers possibly around the heme cleft. The Trp (59) does have a positively charged Lys (60) residue adjacent to it, also the Tyr (74) has a positively charged Lys (73) and Lys (72) at adjacent positions around the heme cleft (Scheme 1B). These residues provide suitable sites for the binding of negatively charged AOT anion thus facilitates the conformational alteration around aromatic residues. Beyond C_1, $-\theta$ of Trp and Tyr residues increased till C_3 with a small inflection around, 0.19 mmol.L^{-1} in the case of Tyr. The $-\theta$, of Phe residue increased right from the monomeric region to C_2. The increase in $-\theta$ of these residues indicates the stabilization of tertiary structure till C_3.The stabilization in the aggregation region may happen due to the duel cross linking of electrostatically attached AOT anion via hydrophobic interactions with the hydrophobic residues around positively charged residues since the hydrophobic interactions does stabilizes the tertiary structure.[2] The hydrophobic forces further increased as the AOT anions aggregates giving ideal opportunity to interact with hydrophobic side chains of various amino acids in the protein backbone thus stabilizing the tertiary structure. In fact the Lys residue itself is having a hydrophobic alkyl chain and have a hydrophobic amino acid isoleucine and leucine at various positions around Trp, Tyr and Phe which themselves are hydrophobic

(Scheme 1B) thus making these interactions feasible. Post $C_3 - \theta$ of Trp, Tyr and Phe decreased thus indicating the loss of tertiary structure due to protein unfolding caused by an increase in nonspecific hydrophobic interactions of the environment around the aromatic residues with the vesicular bilayer. In the vesicle rich region the altered conformation of Cyt c remains stable probably at the interface of AOT head group and bilayers as reported with liposomes of other surfactants.[37-39,48] The tertiary structural changes are abiding the quantitative secondary structural changes of Cyt c, thus indicating the similar effect of [Cho][AOT] both on secondary and tertiary structure of Cyt c in protein backbone. SDS on the other hand has been reported to retain majority of the secondary structure whereas it alters the tertiary structure of Cyt c significantly in the submicellar region.[36] Representative conformational alteration in Cyt c upon [Cho][AOT] binding in various concentration regimes is depicted in Scheme 2.

3.4. Cyt c Conformational analysis from fluorescence correlation spectroscopy

FCS analysis has been utilized to observe the changes in the hydrodynamic radii (R_h) of Cyt c in different concentration regimes.

3.4.1 From monomeric to vesicular regime (0 - 0.4 mmol.L^{-1})

The correlation data obtained from FCS analysis of A488-Cyt c (Fig. S13, ESI†) was fitted to the following model, which consisted of single-component diffusion along with another component representing conformation fluctuation.

$$G(\tau) = \frac{1 - F + F\exp(-\tau/\tau_R)}{N(1-F)}\left(1 + \frac{\tau}{\tau_D}\right)^{-1}\left(1 + \frac{\tau}{\kappa^2 \tau_D}\right)^{-\frac{1}{2}} \quad (1)$$

In the above equation, τ_D is the diffusion time, κ is the structure parameter of the observation volume and is given by $\kappa = \omega_z/\omega_{xy}$, where, ω_z and ω_{xy} are the longitudinal and transverse radii of the observation volume, respectively. τ_R is the relaxation time and F is the associated amplitude. N is the number of fluorescent molecules in the observation volume. Excitation volume was calibrated using Rh6G (Diffusion coefficient 426 $\mu m^2/s$ in water) and found to be 0.8 fL. Diffusion coefficient (D) of the molecule is estimated using equation 2.

$$\tau_D = \frac{\omega_{xy}^2}{4D} \quad (2)$$

The diffusion coefficients were utilized to calculate the hydrodynamic radii of the Cyt c using Stokes Einstein equation.

$$R_h = \frac{k_B T}{6\pi\eta D} \tag{3}$$

The calculated hydrodynamic radii are shown in Fig. 5A. The native Cyt c has the R_h of 1.9±0.1 nm. No significant variation in the R_h of Cyt c was found as it increased only up to 2.2±0.3 nm till C_3, which indicates a very small unfolding after a small initial compaction of protein. The results corroborated well with the variation in all-α secondary structural conformation of Cyt c wherein only small changes in % α-helical content was observed till C_3.

3.4.2 Post vesicular Regime

In vesicular solution we found distortion of the correlation curves due to the association of the Cyt c molecules to vesicles resulting in fluorescence spikes. This problem was circumvented by following a suggested method which involved the collection of several short measurements instead of long measurements.[49] Thus obtained correlation data could be fitted to equation 1 in most cases. In a few cases, we had to use another model (equation 4) involving two diffusion components as shown below

$$\sum_{i=1}^{2} \rho_i \left[1+\frac{\tau}{\tau_i}\right]^{-1} \left[1+\frac{\tau}{\omega^2 \tau_i}\right]^{-1/2} \tag{4}$$

where, ρ_i is given by $\sum_{i=1}^{2} \rho_i = \frac{1}{N}$ and $\rho_i = \frac{\alpha_i}{N}$, α_i is the fraction of molecules with τ_i.

Correlation data along with fits to two-component diffusion model is given in Fig. 5 B. In the vesicular phase (at 1.0 mmol.L^{-1} of [Cho][AOT]) both the models yielded a common diffusion coefficient of 1.7 $\mu m^2\ s^{-1}$ for the Cyt c. In addition, we found a second species (6-10 % fraction) with a diffusion coefficient of 45 μm2 s^{-1} using equation 2. The R_h values corresponding to the two diffusing species are estimated as 125±25 and 5.5±0.3 nm, respectively, which clearly represent Cyt c bound to vesicles and an unfolded state of Cyt c.

3.5. Interactions of cytochrome c with [Cho][AOT] vesicles

Since the Cyt c in the inner membrane of mitochondria interacts with the phospholipid bilayer we investigated the structural changes in [Cho][AOT] vesicles (0.8 to 2 mmol.L^{-1}) upon binding to Cyt c. Fig. 6A shows the zeta potential (ζ) of [Cho][AOT] vesicles and

[Cho][AOT]-Cyt c lipoplexes at different concentrations of [Cho][AOT]. The concentration of Cyt c in the lipoplexes was kept the same (18μM). The ζ of vesicles at different concentrations decreased upon interaction with the Cyt c which indicates electrostatic interactions between the positively charged Lys, Arg or His residues of Cyt c and negatively charged sulphate head group of vesicles. The sizes of [Cho][AOT] vesicles at different concentrations were measured from DLS measurements and are shown in Fig. S14A (ESI†). The corresponding first order intensity autocorrelation functions are shown in Fig. S14B (ESI†). The hydrodynamic diameter of the vesicle was found to be 148 nm. Upon binding with the Cyt c the size of the vesicle decreased from 148 nm to 125 nm in the repeated measurements (Fig. 6B) which indicates the membrane contraction. Since purely electrostatic interactions, leading to surface adsorption are peculiar to globular proteins,[50] the hydrophobic forces of vesicle bilayers with the protein hydrophobic patches[51] must also be playing a role in decreasing the hydrodynamic diameter of the vesicle.[52] Biomembranes in the living body do have the dynamic nature (contraction and expansion) for endo and exocytosis of the molecules.[53-55] The mitochondrial swelling has also been reported upon the release of Cyt c during cell apoptosis.[56] The decrease in size of 3-methyl-1-octylimidazolium vesicles was observed upon binding to protein bovine serum albumin[30] but the vesicles of same surfactant expanded upon binding to protein cellulase.[31] These observations demonstrate the specific nature of proteins[3] and specificity[1] and dynamic nature of vesicular membranes.[53-55] Oxidation of the Cyt c and transition from all-α to α+β secondary structural conformation upon binding with the vesicles has already been discussed earlier. The depiction of Cyt c interaction with [Cho][AOT] vesicles is shown in Scheme 3.

3.6. Peroxidase activity of Cyt c

Fig. 7 shows the changes in absorbance of $ABTS^{\bullet+}$ at 217 nm, formed by Cyt c catalysed oxidation of ABTS and colour change in reaction mixture after 330 seconds at different concentrations of [Cho][AOT]. The corresponding UV-Vis spectra are shown in Fig. S15 (ESI†). Cyt c showed a good peroxidase activity towards the oxidation of ABTS in the presence of H_2O_2[57,58] as indicated by an increase in absorbance at 217 nm due to the formation of $ABTS^{\bullet+}$ radical (Fig. 7). The activity was found to be higher in the presence of [Cho][AOT] as compared to native Cyt c. The reaction rates increased with an increase in concentration of [Cho][AOT] till CVC (0.4 $mmol.L^{-1}$) and decreased slightly in the vesicular regime. Visible changes in the activity of Cyt c were monitored from the changes in the green colour of reaction mixture which showed maximum intensity at CVC (Images, Fig. 7) followed by a slight drop in intensity in the vesicle rich region. An increase in the activity of Cyt c in vesicular solution is due to the higher reaction rates of altered conformation of Cyt c with the H_2O_2 which is the rate determining step of the peroxidase cycle.[58] The increase in peroxidase activity of an artificial enzyme (Au/SiO_2 hetero-nanocomposites) and thermal stability of $ABTS^{\bullet+}$ has been reported in the presence of ILs, [Cho][dhp] and [C_4mim][BF_4].[57] So the all-α to α+β transition of Cyt c upon binding with [Cho][AOT] vesicles is accompanied by an enhancement of peroxidase activity.

4. Conclusion

We conclude our work based on the following points (i) At 298.15 K and pH 7.0 the binding of [Cho][AOT] to Cyt c in monomeric regime is an endothermic process whereas binding in the vesicular regime is an exothermic process wherein the cooperative effect of electrostatic and hydrophobic interactions prevails. (ii) Different conformational alterations were observed around the heme cleft and protein backbone. [Cho][AOT] unfolds Cyt c around the heme cleft till saturation concentration and refolds thereafter in the vesicular and post-vesicular regime as indicated by variation in UV soret band at 409 nm. Disappearance of Q band at 549 nm indicated the oxidation of Cyt c upon binding with [Cho][AOT] bilayers in the post vesicular regime. (iii) [Cho][AOT] destabilizes both secondary and tertiary structure of Cyt c in the protein backbone in the monomeric regime followed by the stabilization of both secondary and tertiary structure till saturation concentration as evidenced from CD spectra. The stabilization in this regime is unusual considering the generalized view of protein destabilization in this regime in surfactant-protein chemistry thus citing the specific nature of Cyt c dedicated to its different folding topology and does find support from its secondary structural stabilization by sub-micelles of SDS.[36] (iv) In vesicular and post-vesicular regime [Cho][AOT] vesicles destabilizes the secondary and tertiary structure of Cyt c. (v) FCS analysis indicated the unfolding of Cyt c upon interaction with [Cho][AOT] vesicles. The binding of Cyt c to [Cho][AOT] vesicular bilayers induced vesicular contraction accompanied by a change in Cyt c conformation from all-α to α+β type protein which is similar to Cyt c binding to mitochondrial inner membrane.[45] (vi) Peroxidase activity of Cyt c increased upon [Cho][AOT] binding in all the concentration regimes with maximum activity observed at critical vesicular concentration. Above findings shows the potential utility of [Cho][AOT] membranes in bio-micking of Cyt c-biomembrane interactions and gives opportunity to explore surface active ionic liquids to understand various biomembrane-protein functions.[1]

Author Information

Corresponding Author

*E-mail: arvind@csmcri.org. Phone: +91-278-2567039. Fax: +91-278-2567562.

Acknowledgements

This work is sponsored by Department of Science and Technology (DST), Government of India under the project No. SB/S1/PC-104/2012. We thank DST also for the FCS facility (obtained under the PURSE Grant) and J.C. Bose Fellowship (to AS). AP thanks CSIR for a Senior Research Fellowship. The analytical division of CSMCRI is acknowledged for sample characterization.

†Electronic supplementary information (ESI) available:

Fig. S1 (CD and UV spectra of native Cyt c), Fig. S2 (^{1}H-NMR spectra of [Cho][AOT] Fig. S3 (DSC thermogram [Cho][AOT]), Fig. S4 (ITC dP plots of [Cho][AOT] aggregation in buffer and Cyt c solution), Fig. S5 (AFM images of [Cho][AOT] vesicles), Fig. S6 ([ChoCl]-Cyt c and [NaAOT]-Cyt c binding isotherms), Fig. S7 (Cyt c UV spectra at various concentrations of [Cho][AOT]), Fig. S8 ([ChoCl]-Cyt c and [NaAOT]-Cyt c UV spectra), Fig. S9 ([Cho][AOT]-Cyt c far UV CD spectra and turn, random coil structural variations), Fig. S10 (variations in the -$\theta_{222\ nm}$ peak), Fig. S11 (Far-UV CD spectra of [ChoCl]-Cyt c and [NaAOT]-Cyt c), Fig. S12 (Mid-UV CD spectra of Cyt c at various concentrations of [Cho][AOT]), Fig. S13 (Correlation data of A488-Cyt c), Fig. S14 (hydrodynamic diameters of [Cho][AOT] vesicles at various concentrations), Fig. S15 (UV-Vis spectra of ABTS at different concentrations of [Cho][AOT]).

References

1. U. H. N. Dürr, M. Gildenberg, A. Ramamoorthy, *Chem. Rev.* 2012, **112**, 6054-6074.
2. D. Otzen, *Biochim. Biophys. Acta* 2011, **1814**, 562-591.
3. M. N. Jones, *Chem. Soc. Rev.* 1992, **21**, 127-136.
4. E. Soussan, S. Cassel, M. Blanzat, I. Rico-Lattes, *Angew. Chem., Int. Ed.* 2009, **48**, 274–288.
5. Y. Barenholz, D. Peer, *Chem. Phys. Lipids* 2012, **165**, 363-364.
6. G. W. Bushnell, G. V. Louie, G. D. Brayer, *J. Mol. Biol.* 1990, **214**, 585-595.
7. G. C. Mills, *J. theor. Biol.* 1991, **152**, 177-190

8. L. Banci, I. Bertini, J. G. Huber, G. A. Spyroulias, P. Turano, *J. Biol. Inor. Chem.* 1999, **4**, 21-31.
9. H. Y. Wang, J. J. Wang, S. B. Zhang, X. P. Xuan, *J. Phys. Chem. B* 2008, **112**, 16682-16689.
10. Y. Zhao, S. J. Gao, J. J. Wang, J. M. Tang, *J. Phys. Chem. B* 2008, **112**, 2031-2039.
11. M. Ao, G. Xu, Y. Zhu, Y. Bai, *J. Colloid Interface Sci.* 2008, **326**, 490-495.
12. B. Chamiot, C. Rizzi, L. Gaillon, J. Sirieix-Plenet, J. Lelievre, *Langmuir* 2009, **25**, 1311-1315.
13. T. Singh, M. Drechsler, A. H. E Müller, I. Mukhopadhyay, A. Kumar, *Phys. Chem. Chem. Phys.* 2010, **12**, 11728-11735.
14. K. S. Rao, T. Singh, T. J. Trivedi, A. Kumar, *J. Phys. Chem. B* 2011, **115**, 13847-13853.
15. K. S. Rao, T. J. Trivedi, A. Kumar, *J. Phys. Chem. B* 2012, **116**, 14363-14374.
16. J. Jingjing, H. Bing, L. Meijia, C. Ni, Y. Li, L. Min, *J. Colloid Interface Sci.* 2013, **412**, 24-30.
17. K. S. Rao, S. So, A. Kumar, *Chem. Commun*. 2013, **49**, 8111-8113.
18. C. Ni, Y., Pengming, W. Tao, S. Xiang, B. Yanhui, G. Yanjun, Y. Li., *J. Phys. Chem. B* 2014, **118**, 2758-2768
19. K. S. Rao, P. S. Gehlot, T. J Trivedi, A. Kumar, *J. Colloids Interface Sci.* 2014, **428**, 267-275.
20. R. Kamboj, P. Bharmoria, V. Chauhan, S. Singh, A. Kumar, V. S. Mithu, T. S Kang. *Langmuir* 2014, **30**, 9920-9930.
21. K. P. Ananthapadmanabhan, E. D. Goddard, *Interactions of Surfactants with Polymers and Proteins*, CRC Press, Inc: London, U. K., **1993**, Chapter 8.
22. M. N. Jones, *Chem. Soc. Rev.* 1992, **21**, 127-136.
23. D. G. Dalgleish, J. Sjoblom, *In Emulsions and Emulsion Stability*, Marcel Dekker, New York, 1996, Chapter 5.
24. F. Geng, L. Zheng, J. Liu, L. Yu, C. Tung, *Colloid Polym. Sci.* 2009, **287**, 1253-1259.
25. F. Geng, L. Zheng, L. Yu, G. Li, C. Tung, *Process Biochem.* 2010, **45**, 306-311.
26. T. Singh, S. Boral, H. B. Bohidar, A. Kumar, *J. Phys. Chem. B*, 2010, **114**, 8441-8448.
27. T. Singh, P. Bharmoria, M. Morikawa, N. Kimizuka, A. Kumar, *J. Phys. Chem. B*, 2012, **116**, 11924-11935.
28. X. Wang, J. Liu, L. Sun, L. Yu, J. Jiao, R. Wang, *J. Phys. Chem. B*, 2012, **116**, 12479-12488.

29. H. Yan, J. Wu, G. Dai, A. Zhong, H. Chen, J. Yang, D. Han, *J. Lumin.*, 2012, **132**, 622-628.
30. P. Bharmoria, K. S. Rao, T. J. Trivedi, A. Kumar, *J. Phys. Chem. B*, 2014, **118**, 115-124.
31. P. Bharmoria, M. J. Mehta, I. Pancha, A. Kumar, *J. Phys. Chem. B*, 2014, **118**, 9890-9899.
32. P. C. A. G. Pinto, D. M. G. P. Ribeiro, A. M. O. Azevedo, V. D. Justina, E. Cunha, K. Bica, M. Vasiloiu, S. Reisa, M. L. M. F. S. Saraiva, *New J. Chem.* 2013, **37**, 4095-4102.
33. C. Cao, J. Lei, L. Zhang, F. P. Du, *Langmuir*, 2014, **30**, 13744-13753.
34. T. Huang, C. Cao, Z. Liu, Y. Li, F.P. Du, *Soft Matter*, 2014, **10**, 6810-6819.
35. L. Gebicka, J. L. Gebicki, *J. Protein Chem.*, 1999, **18**, 165-172.
36. K. Chattopadhyay, S. Mazumdar, *Biochemistry*, 2003, **42**, 14606-14613.
37. M. Rytomaa, P. Mustonen, P. K. J. Kinnunen, *J. Biol. Chem.*, 1992, **267**, 22243-22248.
38. G. P. Gorbenko, J. G. Molotkovsky, P. K.J. Kinnunen, *Biophys. J.*, 2006, **90**, 4093-4103.
39. M. N. Dimitrova, H. Matsumura, N. Terezova, V. Neytchev, *Colloids and Surfaces B*: *Biointerfaces*, 2002, **24**, 53-61.
40. F. Zhang, E. S. Rowe, *Biochim. Biophys. Acta*, 1994, **1193**, 219-225.
41. K. C. Tama, E. W.Jones, *Chem. Soc. Rev.*, 2006, **35**, 693–709
42. H. Tajima, S. Ikeda, M. Matsuda, N. Hanasaki, J. W. Oh, H. Akiyama, *Solid State Commun.*, 2003, **126**, 579-581.
43. T. K. Das, S. Mazumdar, S. Mitra, *Eur. J. Biochem*., 1998, **254**, 662-670.
44. M. Bihari, T. P. Russell, D. A. Hoagland, *Biomacromolecules*, 2010, **11**, 2944-2948.
45. S. M. Kelly, T. J. Jess, N. C. Price, *Biochim. Biophys. Acta*, 2005, **1751**, 119-139.
46. S. R. Martin, M. J. Schilstra, *Methods Cell Biol*, 2008, **84**, 263-293.
47. P. Manavalan, W. C. Jr Johnson, *Nature*, 1983, **305**, 831-832.
48. J. D. Cortese, A. L. Voglino, C. R. Hackenbrock, Biochemistry, 1998, 37, 6402-6409.
49. R. Rigler, E. Elson, Fluorescence Correlation Spectroscopy: Theory and Applications, Springer 2001.
50. A. S. Ladokhin, M. E Selsted, S. H. White, *Biophys. J.* 1997, **72**, 1762-1766.
51. Shai, Y., *Biochim. Biophys. Acta* 1999, **1462**, 55-70.
52. F. Sciscione, C. Pucci, C. L. Mesa, *Langmuir* 2014, **30**, 2810-2819
53. A. Bonito, R. H. Nochetto, M. S. Pauletti, *Math. Model. Nat. Phenom.*, 2011, **6**, 25-43.
54. G. Blobel, B. Dobberstein, *J. Cell Biol.*, 1975, **67**, 835-851
55. D. Görlich, T. A Rapoport, *Cell*, 1993, **75**, 615-630.
56. W. Gao, Y. Pu, K. Q. Luo, D. C, Chang, *J. Cell Sci.* 2001, **114**, 2855-2862.

57. Y. Lin, A. Zhao, Y. Tao, J. Ren, X. Qu, *J. Am. Chem. Soc.* 2013, **135**, 4207–4210.

58. L. Gebicka, *Res. Chem. Intermed.*, 2001, **27**, 717-723.

Scheme 1. (A) Chemical structure of Choline dioctylsulfosuccinate (B) Model structure of amino acid sequence of enzyme cytochrome c[a]

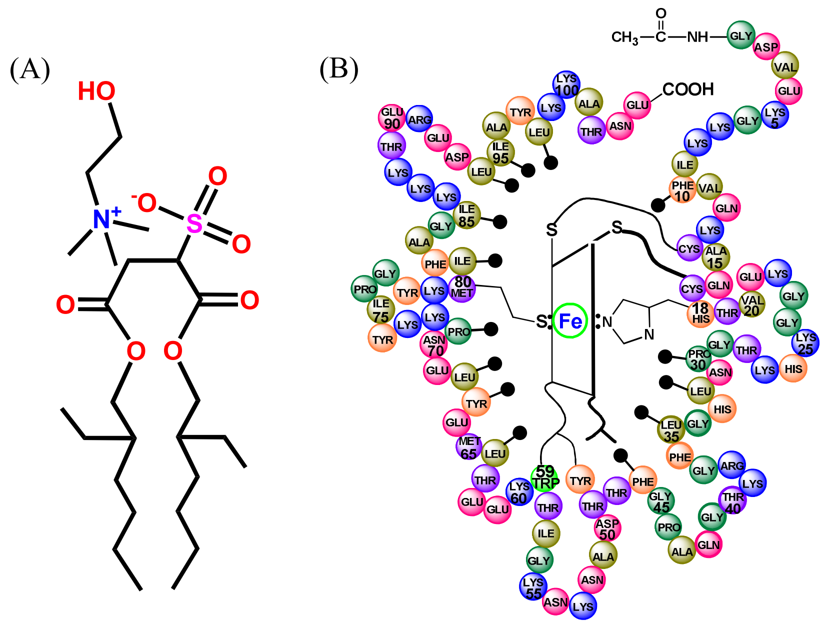

[Cho][AOT] Cytochrome c

[a] The structure has been redrawn from ref. 7 with permission

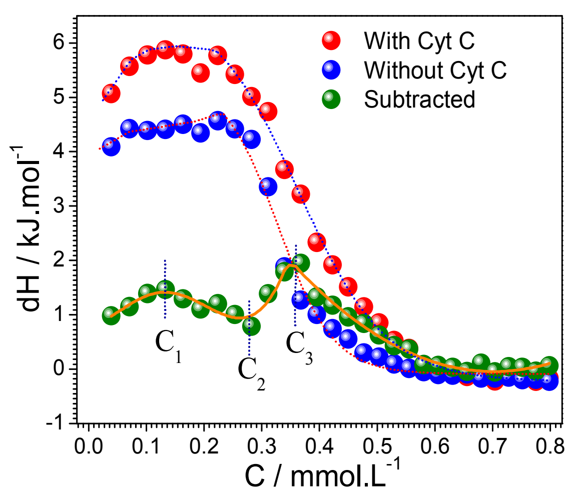

Fig. 1 ITC thermograms of [Cho][AOT] aggregation in buffer, Cytochrome c solution and [Cho][AOT]→Cytochrome c binding isotherm. Lines marking different concentration regimes of [Cho][AOT]-Cytochrome c interaction are discussed in the text.

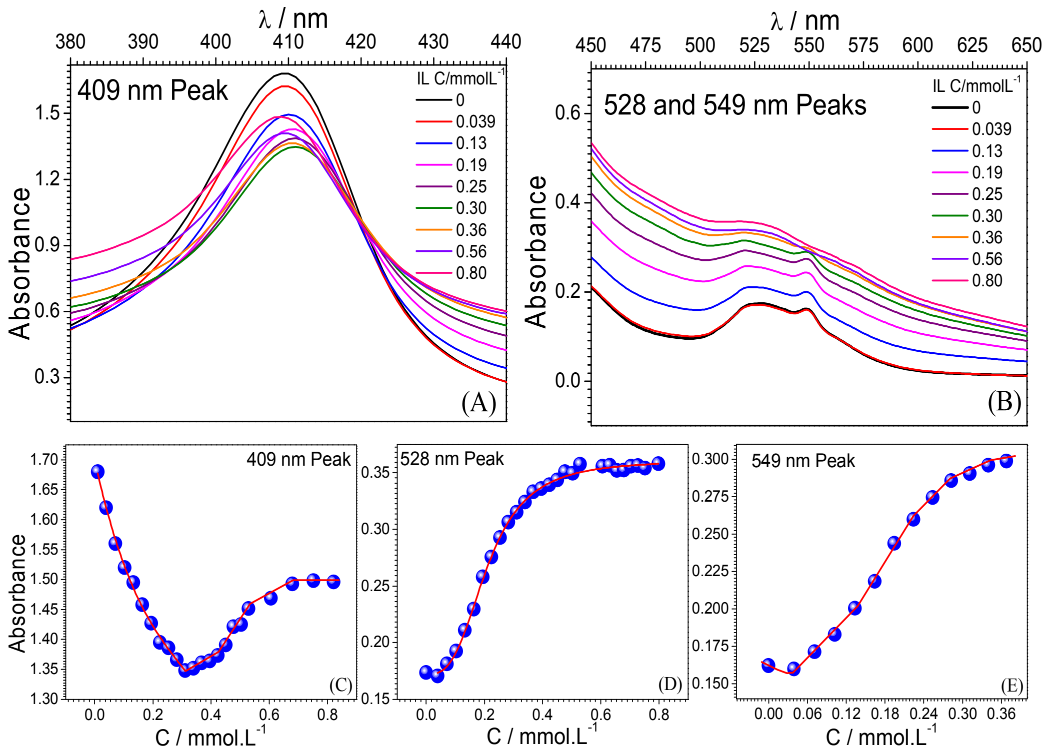

Fig. 2 UV-Vis spectra of Cytochrome c, at different concentrations of [Cho][AOT] showing different absorption wavelengths (A) 409 nm and (B) 528 and 549 nm. (C), (D) and (E) shows the variation in absorption intensity of Cytochrome c at different concentrations of [Cho][AOT].

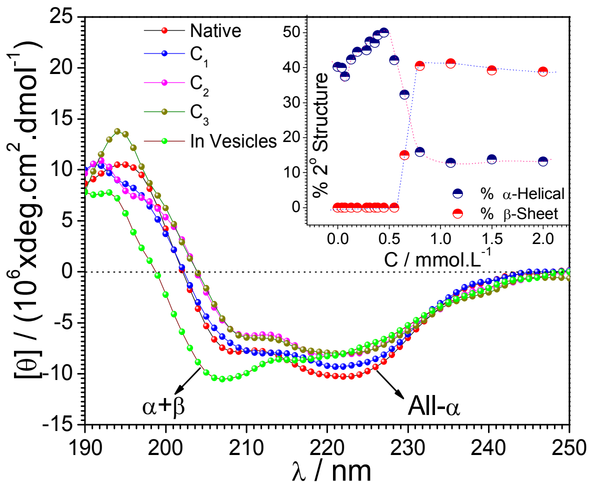

Fig. 3 Far-UV CD spectra of Cytochrome c, at different concentrations of [Cho][AOT]. Inset shows the variation in % α-helical and % β-sheet content of Cytochrome c.

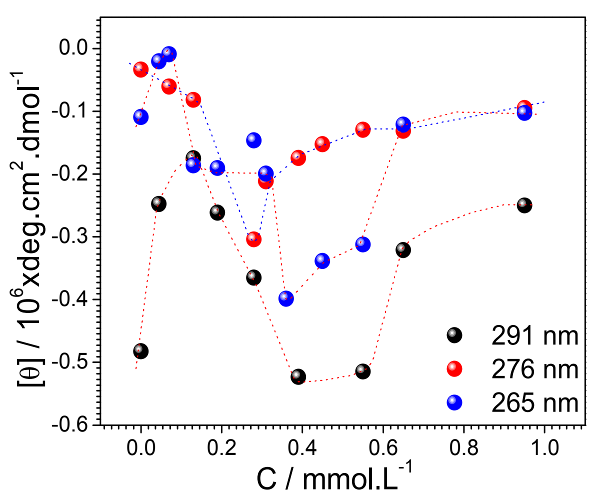

Fig. 4 Mid-UV CD spectra of Cytochrome c, at different concentrations of [Cho][AOT].

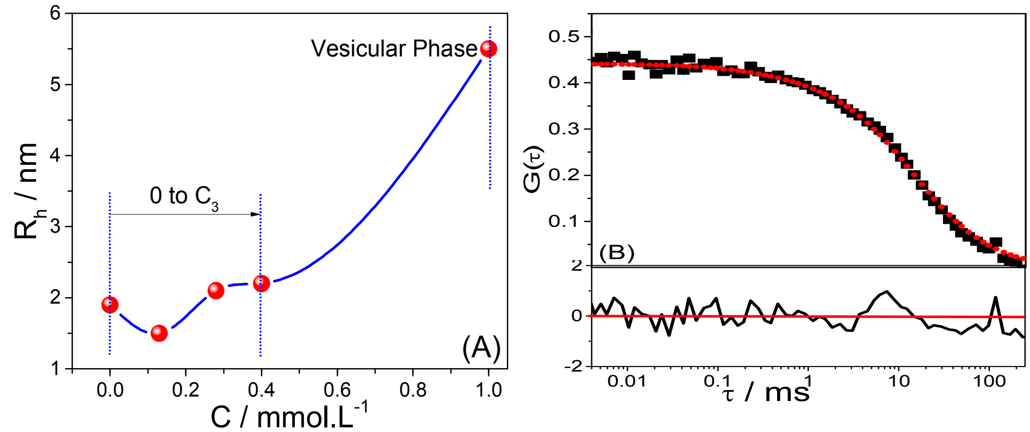

Fig. 5 (A) Variations in the hydrodynamic radii (R_h) of Cytochrome c as a function of [Cho][AOT] concentration.(B) Correlation data along with fits to two-component diffusion model along with conformation fluctuation for A488-Cyt c in 1.0 mmol.L^{-1} of [Cho][AOT] solution.

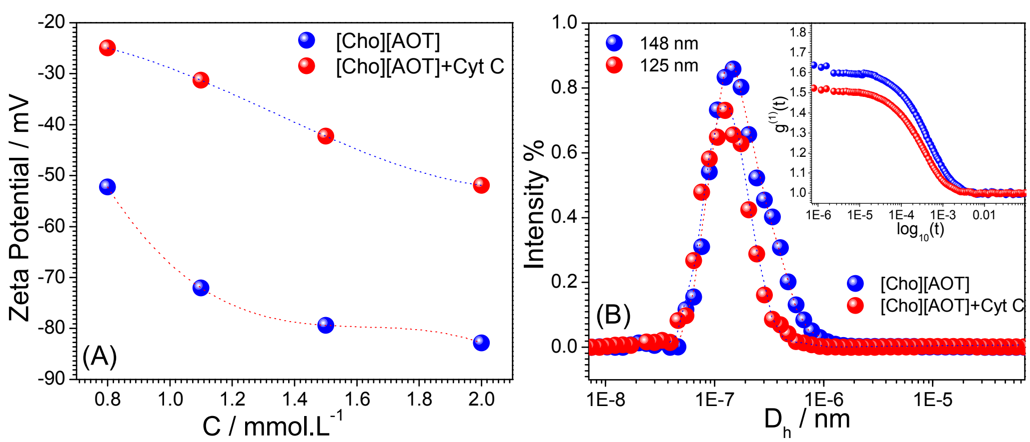

Fig. 6 (A) Zeta potential of [Cho][AOT] vesicles and [Cho][AOT]-Cytochrome c lipoplexes (B) Size of [Cho][AOT] vesicles and [Cho][AOT]-Cytochrome c lipoplexes

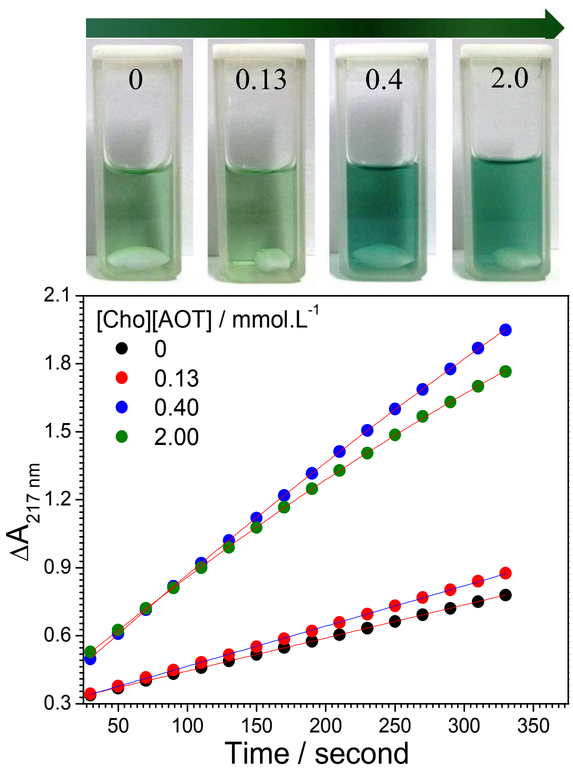

Fig. 7 Changes in the absorbance of ABTS$^{\bullet+}$ upon oxidation at 217 nm as a function of time. Images at the top showing the reaction mixtures after 330 seconds of incubation at different concentration of [Cho][AOT] in mmol.L^{-1}.

Scheme 2. Conformational alteration in cytochrome c in different concentration regime of [Cho][AOT]-cytochrome c system.[a]

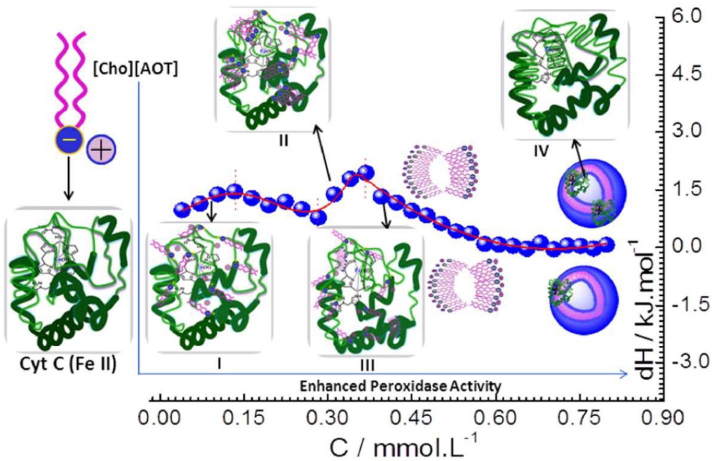

[a] I→ Cyt c-[Cho][AOT] monomeric complex below C_1, II→Cyt c-[Cho][AOT] aggregate complex between C_1 and C_3, III→Oxidised Cytc-[Cho][AOT] complex just above C_3 and IV→Oxidised α+β conformation of Cyt c attached to [Cho][AO]T vesicles.

Scheme 3. Conformational alteration in cytochrome c upon binding to [Cho][AOT] vesicles post CVC.

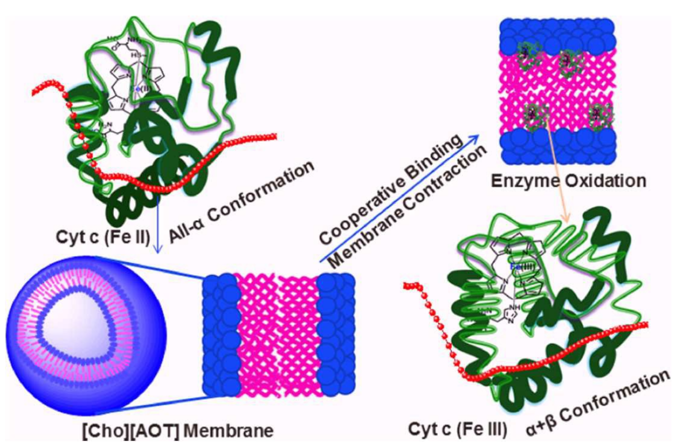

Table 1. Thermodynamic parameters obtained from isothermal titration calorimetry technique at 298.15 K

Sample	*CVC / mmol.L^{-1}*	Parameter		
	I.T.C.	ΔH^{o}_{agg} (kJ.mol^{-1})	$T\Delta S^{o}_{agg}$ (kJ.mol^{-1})	ΔG^{o}_{agg} (kJ.mol^{-1})
[Cho][AOT]+ Buffer	0.34	-4.79	35.78	-40.57
[Cho][AOT]+ 18μM Cyt c	0.40	-6.05	35.18	-41.23

Table 2. Variation in % secondary structure of cytochrome c as function of [Cho][AOT] concentration

[Cho][AOT] Conc. (mmol.L^{-1})	Secondary Structure			
	% α-Helical	% β-Sheet	% Turn	% Random Coil
0	40.2	0.00	27.6	32.2
0.04	40.0	0.00	28.9	31.2
0.07	37.5	0.00	28.2	33.8
0.13	42.3	0.00	26.7	33.5
0.19	44.5	0.00	28.4	27.0
0.28	45.0	0.00	27.3	27.6
0.31	47.5	0.00	28.4	24.0
0.36	47.1	0.00	27.0	25.9
0.39	49.3	0.00	26.0	24.7
0.45	50.0	0.00	24.3	25.7
0.55	42.1	0.00	26.1	31.8
0.65	32.3	15.0	16.6	36.0
0.80	15.9	40.5	7.2	36.3
1.10	12.8	41.2	4.4	41.6
1.50	13.8	39.2	5.7	41.6
2.00	13.2	38.9	6.4	41.6

TOC 300 dpi

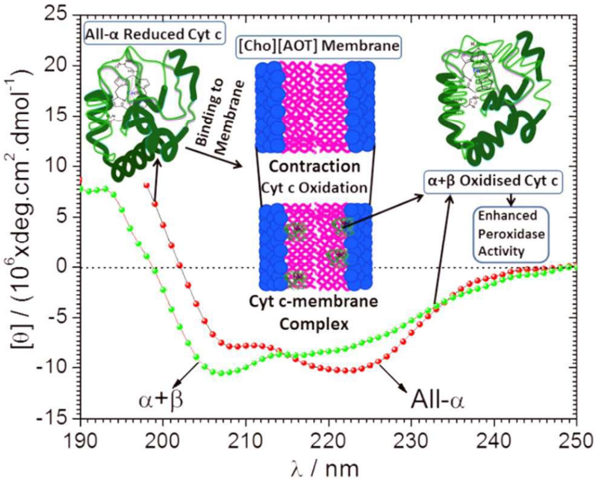

All-α Reduced Cyt c
[Cho][AOT] Membrane
Binding to Membrane
Contraction
Cyt c Oxidation
α+β Oxidised Cyt c
Enhanced Peroxidase Activity
Cyt c-membrane Complex
α+β
All-α
[θ] / (10^6 xdeg.cm^2.dmol^-1)
λ / nm